I R A M P
4(2), December 2013, pp. 105-119

ISSN: 2229-3159

Aspects of Lorentz-Stark Broadening of Hydrogen Spectral Lines in Magnetized, Turbulent and Non-Turbulent Plasmas Important for Magnetic Fusion and Solar Physics

E. OKS[1]

[1]*Physics Department, 206 Allison Lab, Auburn University, Auburn, AL 36849, USA*

ABSTRACT: Broadening of hydrogen spectral lines in plasmas is an important diagnostic tool for many applications (here and below by "hydrogen atoms" and "hydrogen spectral lines" we mean atoms and spectral lines of hydrogen, deuterium, and tritium). In magnetized plasmas radiating hydrogen atoms moving with the velocity **v** across the magnetic field **B** experience a Lorentz electric field $\mathbf{E}_L = \mathbf{v} \times \mathbf{B}/c$ in addition to other electric fields. Since the velocity **v** has a distribution, so does the Lorentz field, thus making an additional contribution to the broadening of spectral lines. Compared to previous studies of this contribution, we cover the following new aspects. First, we consider magnetized plasmas containing a low-frequency electrostatic turbulence. We derive analytically distributions of the total electric field and the corresponding Stark profiles of hydrogen lines. Second, for non-turbulent magnetized plasmas we derive analytically Lorentz-broadened profiles of highly-excited hydrogen lines. We obtain formulas for the principal quantum number n_{max} of the last observable hydrogen line in the spectral series. These formulas differ very significantly from the corresponding Inglis-Teller result and constitute a new diagnostic method allowing to measure the product $T^{1/2}B$, where T is the atomic temperature. Third, we discuss the Lorentz-Doppler broadening of highly-excited hydrogen lines and produce new analytical results. We demonstrate that our findings lead to a significantly revised interpretation of the previous and future experimental data in magnetic fusion and the observational data in solar physics.

PACS Numbers: 32.70.Jz, 32.60. + i, 52.25.Xz, 52.55.Jd, 96.60.-j.

1. INTRODUCTION

Broadening of hydrogen spectral lines in plasmas is an important diagnostic tool for many applications (here and below by "hydrogen atoms" and "hydrogen spectral lines" we mean atoms and spectral lines of hydrogen, deuterium, and tritium). In magnetized plasmas radiating hydrogen atoms moving with the velocity **v** across the magnetic field **B** experience a Lorentz electric field $\mathbf{E}_L = \mathbf{v} \times \mathbf{B}/c$ in addition to other electric fields. Since the velocity **v** has a distribution, so does the Lorentz field, thus making an additional contribution to the broadening of spectral lines. In 1970, Galushkin [1] considered a joint effect of Lorentz and Doppler broadenings (including also Zeeman splitting) and produced many interesting analytical results. He noted, in particular, that Lorentz and Doppler broadenings cannot be accounted for via a convolution, but rather they intertwine in a more complicated manner.

In the intervening decades other authors also contributed to the subject [2-6]. However, first, the scope of papers [1-6] was limited to some spectral lines originating from levels of the principal quantum number n = 2, 3, or 4, namely Ly_α, H_α, and H_β lines of hydrogen in [1-3, 5, 6] and Ly_α of C VI in [4]. Second, electrostatic turbulence, which frequently occurs in various kinds of laboratory and astrophysical plasmas [7, 8] and which affects transport phenomena in magnetized plasmas [9], was not taken into account in [1-6].

In the present paper we cover the following new aspects. First, we consider magnetized plasmas containing a low-frequency electrostatic turbulence. This kind of turbulence causes anomalous transport phenomena (e.g., the anomalous resistivity) and is therefore very important to be diagnosed. We derive analytically distributions of the

total electric field and the corresponding Stark profiles of hydrogen lines. Second, for non-turbulent magnetized plasmas we derive analytically Lorentz-broadened profiles of highly-excited hydrogen lines. We obtain expressions for the principal quantum number n_{max} of the last observable hydrogen line in the spectral series. These expressions differ very significantly from the corresponding Inglis-Teller result [10] and constitute a new diagnostic method allowing to measure the product $T^{1/2}B$, where T is the atomic temperature. Third, we discuss the Lorentz-Doppler broadening of highly-excited hydrogen lines and produce new analytical results. We demonstrate that our findings lead to a significantly revised interpretation of the previous and future experimental data in magnetic fusion and the observational data in solar physics.

2. TOTAL ELECTRIC FIELD DISTRIBUTIONS IN TURBULENT MAGNETIZED PLASMAS AND THE CORRESPONDING STARK PROFILES OF HYDROGEN LINES

At the absence of a magnetic field, there is only one type of a low-frequency electrostatic turbulence: ion acoustic waves – frequently called *ionic sound*. The corresponding oscillatory electric field is a broadband field, whose frequency spectrum is below or of the order of the ion plasma frequency

$$\omega_{pi} = (4\pi e^2 N_i Z^2/m_i)^{1/2} = 1.32 \times 10^3 Z (N_i m_p/m_i)^{1/2}, \quad (1)$$

where N_i is the ion density, Z is the charge state; m_p and m_i are the proton and ion masses, respectively. In the "practical" parts of this and subsequent equations, CGS units are used unless specified to the contrary.

In magnetized plasmas in addition to the ionic sound, propagating along the magnetic field **B**, two other types of low-frequency electrostatic turbulence are possible. One is *electrostatic ion cyclotron wave*, whose wave vector is nearly perpendicular to **B**. Its frequency is close to the ion cyclotron frequency

$$\omega_{ci} = ZeB/(m_i c) = 9.58 \times 10^3 ZB (m_p/m_i)^{1/2} \quad (2)$$

or to its harmonics (*Bernstein modes*). Another type is *lower hybrid oscillations* having the wave vector perpendicular to **B**. Its frequency is

$$\omega = 1/[(\omega_{ci}\, \omega_{ce})^{-1} + (\omega_{pi})^{-2}]^{1/2}, \quad (3)$$

where ω_{ce} is the electron cyclotron frequency

$$\omega_{ci} = eB/(m_e c) = 1.76 \times 10^7 B. \quad (4)$$

From Eq. (3) it is seen that $\omega < \omega_{pi}$ always. This means that frequencies of both ionic sound and lower hybrid oscillations are below or of the order of the ion plasma frequency ω_{pi}.

Usually hydrogenic radiators perceive oscillatory electric fields, associated with a low-frequency plasma turbulence as *quasistatic*. More details on this can be found in review [11], Sect. 5.

The average turbulent electric field $<E_t>$ can significantly exceed the average ion microfield $<E_i>$ in weakly coupled (a.k.a. ideal) plasmas. These are plasmas where there is a large number of ions n_D in the sphere of the Debye radius:

$$n_D = [T_e^3/(36\pi N_e e^6)]^{1/2} = 1377\, [T_e^3/N_e)]^{1/2} >> 1 \quad (5)$$

(here T_e is the electron temperature in Kelvin). In these plasmas the ion microfield can be described by the Holtsmark distribution [12] characterized by the so-called Holtsmark field

$$E_0 = 2.603\, eN_e^{2/3} = 1.25 \times 10^{-9}\, N_e^{2/3}. \quad (6)$$

In this case the most probable ion field is

$$E_{i\,max} = 1.608\, E_0. \quad (7)$$

The energy density of the turbulent field $<E_t^2>/(16\pi N_e T_e)$ can reach values ~ 0.1, so that the ratio $<E_t>/E_{i\,max}$ can be as high as

$$< E_t > / E_{i\,\max} \sim n_D^{1/3} >> 1, \tag{8}$$

where n_D is given by Eq. (5). For example, for edge plasmas of tokamaks, such as a low-density discharge in Alcator *C*-Mod [13], where $N_e \sim 3 \times 10^{13}$ cm^{-3} and $T \sim 5 \times 10^4$ *K*, one can get $< E_t > / E_{i\,\max} \sim 20$. We note that such a strong low-frequency electrostatic turbulence had been detected via a spectroscopic diagnostic, e.g., in tokamak T-10 [14].

The average Lorentz field

$$< E_L > = B v_T / c = 4.28 \times 10^{-3}\, B [T(K)]^{1/2} \tag{9}$$

(v_T is the atomic thermal velocity) also can exceed the most probable ion microfield E_i when the magnetic field B exceeds the following critical value:

$$B_c = 4.69 \times 10^{-7}\, N_e^{2/3} / [T(K)]^{1/2}, \tag{10}$$

(in Eqs. (9) and (10), B is in Tesla and the atomic temperature T is in Kelvin). For example, in the solar chromosphere the typical plasma parameters are $N_e \sim 10^{11}$ cm^{-3} and $T \sim 10^4$ *K* (except solar flares where N_e can be higher by two orders of magnitude) – see, e.g., [15, 16]. In this case from Eq. (10) we get $B_c = 0.2$ Tesla. A more accurate estimate for this example can be obtained by taking into account that non-thermal velocities $v_{\rm nonth}$ in the solar chromosphere can be ~ several tens of km/s, so that the total velocity $v_{\rm tot} = (v_T^2 + v_{\rm nonth}^2)^{1/2} \sim (15 - 30)$ km/s. Then $E_L = E_{i\,\max}$ already at $B \sim 0.05$ Tesla, while B can reach 0.4 T in sunspots.

Another example is edge plasmas of tokamaks. For a low-density discharge in Alcator *C*-Mod [13], where $N_e \sim 3 \times 10^{13}$ cm^{-3} and $T \sim 5 \times 10^4$ K, we get $B_c = 4$ Tesla, while the actual magnetic field was 8 Tesla.

For completeness we analyze the ratio of the Zeeman width of hydrogen lines $\Delta\omega_Z$ to the corresponding "halfwidth" of the n-multiplet due to the Lorentz broadening $\Delta\omega_L$

$$\Delta\omega_Z = eB/(2 m_e c), \qquad \Delta\omega_L = 3n(n-1)\hbar B v_T/(2 m_e e c), \qquad \Delta\omega_Z/\Delta\omega_L = 5680/[n(n-1)T^{1/2}], \tag{11}$$

where n is the principal quantum number of the upper level involved in the radiation transition and the atomic temperature T is in Kelvin. For example, for the typical temperature at the edge plasmas of tokamaks $T \sim 5 \times 10^4$ K, Eq. (11) yields $\Delta\omega_Z/\Delta\omega_L = 25.4/[n(n-1)]$: so that the Lorentz width exceeds the Zeeman width for hydrogen lines of $n > 5$, while Balmer lines up to $n = 16$ were observed, e.g., at Alcator *C*-Mod [13]. Another example: for the typical temperature in the solar chromosphere $T \sim 10^4$ *K*, Eq. (11) yields $\Delta\omega_Z/\Delta\omega_L = 56.8/[n(n-1)]$. So, the Lorentz width exceeds the Zeeman width for hydrogen lines of $n > 8$, while Balmer lines up to $n \sim 30$ were observed [15, 16].

Thus, we encounter the situations where the two primary broadening mechanisms of hydrogen lines are low-frequency electrostatic turbulence and the Lorentz broadening. In these situations, the shape of hydrogen lines is controlled by the distribution $W(\mathbf{E})$ of the total electric field $\mathbf{E} = \mathbf{E}_t + \mathbf{E}_L$.

In magnetized plasmas the distribution of the turbulent field $W_t(\mathbf{E}_t)$ should be axially symmetric, the axis of symmetry being along the magnetic field. It is Sholin-Oks' distribution [17] of the following form

$$W_t(E_t, \cos\theta)\, dE_t\, d(\cos\theta) = [4/(\pi E_{\rm par}^2)]^{1/2} (E_t^2/E_{\rm perp}^2) \exp\left[-E_t^2/E_{\rm perp}^2 - \cos^2\theta\,(E_t^2/E_{\rm par}^2 - E_t^2/E_{\rm perp}^2)\right] dE\, d(\cos\theta), \tag{12}$$

where $E_{\rm par}$ and $E_{\rm perp}$ are the root-mean-square values of the turbulent field components parallel and perpendicular to **B**, respectively; θ is the angle between **E** and **B**.

The Lorentz field $\mathbf{E}_L$ is confined in the plane perpendicular to **B** where it has the following distribution

$$W_L(E_L)\, dE_L = (2E_L/E_{LT}^2) \exp(-E_L^2/E_{LT}^2)\, dE_L, \qquad E_{LT} = v_T B/c, \qquad v_T = (2T/M)^{1/2}. \tag{13}$$

Here E_{LT} is the average Lorentz field expressed via the thermal velocity v_T of the radiating atoms of mass M. The distribution W_L actually reproduces the shape of the two-dimensional Maxwell distribution of atomic velocities in the plane perpendicular to **B**. This is because the absolute value of the Lorentz field $\boldsymbol{E}_L = \mathbf{v} \times \mathbf{B}/c$ is $E_L = v_R B/c$, where v_R is the component of the atomic velocity perpendicular to **B**.

The distribution $W(\mathbf{E})$ of the total electric field $\mathbf{E} = \mathbf{E}_t + \mathbf{E}_L$ is a convolution of the distributions from Eqs. (12) and (13). In the general case the resulting formula is too cumbersome. Therefore below we focus at two practically important particular cases.

The first case is where the distribution of the turbulent field has the shape of a very *prolate* spheroid, so that essentially it's the following one-dimensional distribution along **B**:

$$W_{t1}(E_t)\,dE_t = (2/\pi)^{1/2}(1/E_{\rm par})\exp[-E_t^2/(2E_{\rm par}^2)]\,dE_t. \tag{14}$$

This situation is typical for the ion acoustic turbulence. The corresponding convolution with the Lorentz field distribution has the form

$$W_1(E,\cos\theta)\,dE\,d(\cos\theta) = dE\,d(\cos\theta)\int_0^\infty dE_L W_L(E_L)$$
$$\int_0^\infty dE_t W_{t1}(E_t)\,\delta[\cos\theta - E_t/(E_t^2+E_L^2)^{1/2}]\delta[E-(E_t^2+E_L^2)^{1/2}] \tag{15}$$

After using the two δ-functions to perform the two integrations, the result reduces to the following:

$$W_1(E,\cos\theta)\,dE\,d(\cos\theta) = dE\,d(\cos\theta)\;W_L(E|\sin\theta|)\,W_{t1}(E\cos\theta)\,E/|\sin\theta|. \tag{16}$$

Based on the total field distribution from Eq. (16), the profiles $S(\Delta\omega)$ of hydrogen lines can be calculated as follows.

$$S(\Delta\omega) = S_\pi(\Delta\omega) + S_\sigma(\Delta\omega), \tag{17}$$

$$S_\pi(\Delta\omega) = \sum_{(\alpha,\beta)\pi}[J_{\alpha\beta}/(k|X_{\alpha\beta}|)]\int_0^1 d(\cos\theta)\;f_\pi(\cos\theta)\,W_1[\Delta\omega/(k|X_{\alpha\beta}|),\cos\theta], \tag{18}$$

$$S_\sigma(\Delta\omega) = \sum_{(\alpha,\beta)\sigma}[J_{\alpha\beta}/(k|X_{\alpha\beta}|)]\int_0^1 d(\cos\theta)\;f_\sigma(\cos\theta)\,W_1[\Delta\omega/(k|X_{\alpha\beta}|),\cos\theta]. \tag{19}$$

Here

$$k = 3\hbar/(2m_e e), \quad X_{\alpha\beta} = n_\alpha(n_1-n_2)_\alpha - n_\beta(n_1-n_2)_\beta, \tag{20}$$

where n_1, n_2 are the parabolic quantum numbers, and n is the principal quantum numbers of the upper (subscript α) and lower (subscript β) Stark sublevels involved in the radiative transition; $J_{\alpha\beta}$ is the relative intensity of the corresponding Stark component. In Eq. (18) the summation is performed over π-components, in Eq. (19) – over σ-components.*/

The functions $f_\pi(\cos\theta)$ and $f_\sigma(\cos\theta)$ in Eqs. (18), (19) depend on the direction of observation. For the observation parallel to **B**:

$$f_\pi(\cos\theta) = (1-\cos^2\theta), \qquad f_\sigma(\cos\theta) = (1+\cos^2\theta)/2. \tag{21}$$

For the observation perpendicular to **B**:

$$f_\pi(\cos\theta) = (1+\cos^2\theta)/2, \qquad f_\sigma(\cos\theta) = (3-\cos^2\theta)/4. \tag{22}$$

*/ For hydrogen lines having the component of $X_{\alpha\beta} = 0$ (which is usually the σ-component), the sum in (19) should be complemented by $J_0\delta(\Delta\omega)$, where J_0 is the relative intensity of the component. Physically this means that the contribution of this component to the overall profile is controlled by other broadening mechanisms (typically, by the Doppler broadening). However, first, for 50% of hydrogen lines, such as those with even values of $(n_\alpha - n_\beta)$, there is no component of $X_{\alpha\beta} = 0$. Second, for high-n hydrogen lines ($n_\alpha >> n_\beta$) with odd values of $(n_\alpha - n_\beta)$, the contribution of this component to the overall profile is relatively small and can be neglected.

Now we consider the second practically important case is where the distribution of the turbulent field has the shape of a very *oblate* spheroid, so that essentially it's the following two-dimensional distribution in the plane perpendicular to **B**:

$$W_{t2}(E_t)\,dE_t = (2E_t/E_{\text{perp}}^2)\exp[-E_t^2/E_{\text{perp}}^2)]\,dE_t. \tag{23}$$

This situation is typical for the Bernstein modes. Obviously in this case the total electric field $\mathbf{E} = \mathbf{E}_t + \mathbf{E}_L$ is confined in the plane perpendicular to **B**. Its distribution has the form:

$$W_2(E)\,dE = dE\,(1/\pi)\int_0^\infty dE_L W_L(E_L)\int_0^\infty dE_t W_{t2}(E_t)\int_0^\pi d\psi\,\delta[E-(E_t^2+E_L^2+2E_tE_L\cos\psi)^{1/2}]. \tag{24}$$

After using the δ-function to perform the integration over the angle ψ (which is the angle between vectors $\mathbf{E}_t$ and $\mathbf{E}_L$), the result reduces to the following:

$$W_2(E)\,dE = dE\,(E/\pi)\int_0^\infty dE_t W_{t2}(E_t)\int_{E_{\min}}^{E_{\max}} dE_L W_L(E_L)/\{[(E_t+E_L)^2-E^2][E^2-(E_t-E_L)^2]\}^{1/2}, \tag{25}$$

where the lower and upper limits of the integration over E_L are

$$E_{\min} = E - E_t, \qquad E_{\max} = E + E_t. \tag{26}$$

Based on the total field distribution from Eq. (25), the profiles $S(\Delta\omega)$ of hydrogen lines can be calculated as follows.

$$S(\Delta\omega) = S_\pi(\Delta\omega) + S_\sigma(\Delta\omega), \tag{27}$$

$$S_\pi(\Delta\omega) = \sum_{(\alpha,\beta)\pi}[J_{\alpha\beta}/(k|X_{\alpha\beta}|)]\,f_\pi W_2[\Delta\omega/(k|X_{\alpha\beta}|)], \tag{28}$$

$$S_\sigma(\Delta\omega) = \sum_{(\alpha,\beta)\pi}[J_{\alpha\beta}/(k|X_{\alpha\beta}|)]\,f_\sigma W_2[\Delta\omega/(k|X_{\alpha\beta}|)]. \tag{29}$$

Here for the observation parallel to **B**

$$f_\pi = 1, \qquad f_\sigma = 1/2, \tag{30}$$

while for the observation perpendicular to **B**

$$f_\pi = 1/2, \qquad f_\sigma = 3/4. \tag{31}$$

We note for completeness that, while the argument of the line profiles in Eqs. (17)-(19) and (27)-(29) is the detuning $\Delta\omega$ from the unperturbed frequency ω_0 of the spectral line, the corresponding profiles in the wavelength scale $S(\Delta\lambda)$, i.e., where the argument is the detuning from the unperturbed wavelength of the spectral line, can be obtained from the same Eqs. (17)-(19) and (27)-(29) by changing the constant $k = 3\hbar/(2m_e e)$ in Eq. (20) to

$$k_0 = [3\hbar/(2m_e e)]\,\lambda_0^2/(2\pi c), \tag{32}$$

where λ_0 is the unperturbed wavelength.

3. LORENTZ-BROADENED PROFILES OF HIGHLY-EXCITED HYDROGEN LINES AND A REVISION OF THE INGLIS-TELLER DIAGNOSTIC METHOD

In non-turbulent magnetized plasmas, the Lorentz broadening can predominate over other broadening mechanisms for highly-excited hydrogen lines. In the previous section we showed that the Lorentz broadening can significantly exceed the Zeeman splitting for high-*n* hydrogen lines. Now let us estimate the ratio of the Lorentz and Doppler broadenings.

The Doppler Full Width and Half Maximum (FWHM) is

$$(\Delta\omega_D)_{1/2} = 2(\ln 2)^{1/2}\,\omega_0 v_T/c = 1.665\,\omega_0 v_T/c, \tag{33}$$

where ω_0 is the unperturbed frequency of the spectral line. For highly-excited hydrogen lines, where $n_\alpha >> n_\beta$, one can use the expression $\omega_0 = m_e e^4/(2n_\beta^2 \hbar^3)$.

The Lorentz-broadened profile of a Stark component of a hydrogen line reproduces the shape of the Lorentz field distribution from Eq. (13)

$$S_{\alpha\beta}(\Delta\omega) = (2\Delta\omega/\Delta\omega_{L\alpha\beta}^2)\exp(-\Delta\omega^2/\Delta\omega_{L\alpha\beta}^2), \quad \Delta\omega_{L\alpha\beta} = kX_{\alpha\beta} B v_T/c. \tag{34}$$

Its FWHM is

$$(\Delta\omega_{L\alpha\beta})_{1/2} = 2.715\,\Delta\omega_{L\alpha\beta}. \tag{35}$$

The corresponding FWHM $(\Delta\omega_L)_{1/2}$ of the entire hydrogen line can be estimated by using in Eqs. (34), (35) the average value $<k|X_{\alpha\beta}|> = (n_\alpha^2 - n_\beta^2)\,\hbar/(m_e e)$, which for $n_\alpha >> n_\beta$ becomes $<k|X_{\alpha\beta}|> = n_\alpha^2\,\hbar/(m_e e)$. Therefore, for the ratio of the FWHM by these two broadening mechanisms we get

$$(\Delta\omega_L)_{1/2}/(\Delta\omega_D)_{1/2} = n_\alpha^2 n_\beta^2 B(\text{Tesla})/526. \tag{36}$$

We note that this ratio does not depend on the temperature.

For Balmer lines ($n_\beta = 2$) Eq. (36) becomes

$$(\Delta\omega_L)_{1/2}/(\Delta\omega_D)_{1/2} = n_\alpha^2 B(\text{Tesla})/131. \tag{37}$$

So, e.g., for the egde plasmas of tokamaks, where Balmer lines of $n_\alpha \sim (10 - 16)$ have been observed, the Lorentz broadening dominates over the Doppler broadening when the magnetic field exceeds the critical value $B_c \sim 1$ Tesla. This condition is fulfilled in the modern tokamaks and will be fulfilled also in the future tokamaks.

Another example: in solar chromosphere, where Balmer lines of $n_\alpha \sim (25 - 30)$ have been observed, the Lorentz broadening dominates over the Doppler broadening when the magnetic field exceeds the critical value $B_c \sim (0.15 - 0.2)$ Tesla. This condition can be fulfilled in sunspots where B can be as high as 0.4 Tesla.

Therefore it is practically useful to calculate Lorentz-broadened profiles of highly-excited Balmer lines. To ensure that for each particular hydrogen line, the profile will be *universal*, i.e., applicable for any B and T, we chose the argument γ of the profiles as

$$\gamma = c\,\Delta\omega/(kBv_T). \tag{38}$$

We calculated the corresponding profiles as follows:

$$P(\gamma) = P_\pi(\gamma) + P_\sigma(\gamma), \tag{39}$$

$$P_\pi(\gamma) = \sum_{(\alpha,\beta)\pi} (J_{\alpha\beta}/|X_{\alpha\beta}|)\, f_\pi\, W(\gamma/|X_{\alpha\beta}|), \tag{40}$$

$$P_\sigma(\gamma) = \sum_{(\alpha,\beta)\sigma} (J_{\alpha\beta}/|X_{\alpha\beta}|)\, f_\sigma\, W(\gamma/|X_{\alpha\beta}|), \tag{41}$$

where

$$W(u) = 2u\exp(-u^2) \tag{42}$$

(Eq. (42) is the renormalized Eq. (13)). The quantities f_π, f_σ in Eqs. (40), (41) are given by Eq. (30) for the observation parallel to **B** or by Eq. (31) for the observation perpendicular to **B**, respectively.

As an example, Fig. 1 presents calculated universal Lorentz-broadened profiles of the Balmer line H_{18} for the observations perpendicular to **B** (solid line) and parallel to **B** (dashed line).

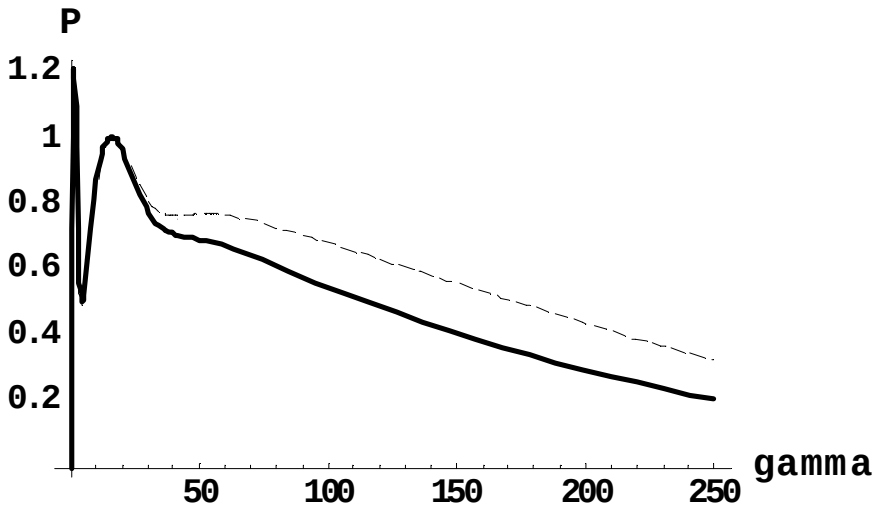

Figure 1: Calculated universal Lorentz-broadened profiles $P(\gamma)$ of the Balmer line H_{18} for the observations perpendicular to B **(solid line) and parallel to** B **(dashed line). The argument $\gamma = c\,\Delta\omega/(kBv_T)$, where $k = 3\hbar/(2\,m_e e)$. The intensities of both profiles are relative to the intensity of the 2nd maximum (whose intensity is set as unity). The 1st maximum would be smeared out by the Doppler broadening**

The resulting extensive tables of the universal profiles $P(\gamma)$ of hydrogen lines will be published elsewhere. Here we present the following practically important result derived from these tables for highly excited Balmer lines.

For any two adjacent high-n Balmer lines (such as, e.g., H_{16} and H_{17}, or H_{17} and H_{18}), the sum of their half widths at half maximum in the frequency scale, the sum being denoted here simply as $\Delta\omega_{1/2}$, turned out to be

$$\Delta\omega_{1/2} = A\,[3n^2\,\hbar\,Bv_T/(2\,m_e ec)], \tag{43}$$

where the constant A depends on the direction of observation as follows:

$$A = 0.80 \text{ (observation perpendicular to } \mathbf{B}) \tag{44}$$

$$A = 1.00 \text{ (observation parallel to } \mathbf{B}), \tag{45}$$

$$A = 0.86 \text{ (“isotropic” observation).} \tag{46}$$

Here by the “isotropic” observation we describe the situation where along the line of sight there are regions with various directions of the magnetic field, which could be sometimes the case in astrophysics.

The results presented in Eqs. (43)-(46) lead to a revision of the diagnostic method based on the principal quantum number $n_{\max}$ of the last observed line in the spectral series of hydrogen lines, such as, e.g., Lyman, or Balmer, or Paschen lines (though typically Balmer lines are used). This method was first proposed by Inglis and Teller [10]. The idea of the method was that the Stark broadening of hydrogen lines by the ion microfield (in case it is quasistatic) in the spectral series scales as $\sim n^2$. Therefore, at some value $n = n_{\max}$, the sum of the Stark half widths at half maximum of the two adjacent lines becomes equal to the unperturbed separation of these two lines, so that they (and the higher lines) merge into a quasicontinuum. Since the Stark broadening is controlled by the ion density N_i (equal to the electron density N_e for hydrogen plasmas), this had led previously to the following simple reasoning.

At the electric field E, for the multiplet of the principal quantum number $n >> 1$, the separation $\Delta\omega(n)$ of the most shifted Stark sublevel from the unperturbed frequency $\omega_0(n)$ is $\Delta\omega(n) = 3n^2\,\hbar\,E/(2\,m_e e)$. Then the sum of the “halfwidths” of the two adjacent Stark multiplets of the principal quantum numbers n and $n + 1$ is

$$\Delta\omega_{1/2}(n) = 3n^2\,\hbar\,E/(m_e e). \tag{47}$$

The unperturbed separation (in the frequency scale) between the hydrogen spectral lines, originating from the highly-excited levels n and $n + 1$ is

$$\omega_0(n + 1) - \omega_0(n) = m_e e^4/(n^3 \hbar^3). \tag{48}$$

By equating (47) and (48) one finds

$$n_{\max}^5 E = E_{at}/3 = 1.714 \times 10^7 \text{ CGS}, \quad E_{at} = m^2 e^5/\hbar^4 \tag{49}$$

($E_{at} = 1.714 \times 10^7$ CGS $= 5.142 \times 10^9$ V/cm is the atomic unit of electric field). For the field E, Inglis and Teller [10] used the most probable field of the Holtsmark distribution, which they estimated as $E_{\max.} = 3.7\, eN_i^{2/3} = 3.7\, eN_e^{2/3}$, and obtained from Eq. (49) the following relation:

$$N_e n_{\max}^{15/2} = 0.027/a_0^3 = 1.8 \times 10^{23} \text{ cm}^{-3}, \tag{50}$$

where a_0 is the Bohr radius. We note that Hey [18], by using a more accurate value of the most probable Holtsmark field $E_{\max} = 4.18\, eN_e^{2/3}$, obtained a slightly more accurate numerical constant in the right side of Eq. (50), namely $0.0225/a_0^3$, while Griem [19] suggested this constant to be even twice smaller.

Thus, Inglis-Teller relation (50) constituted a simple method for measuring the electron density by the number $n_{\max}$ of the observed lines of a hydrogen spectral series. The simplicity of this method is the reason why, despite the existence of more sophisticated (but more demanding experimentally) spectroscopic methods for measuring N_e, this method is still used in both laboratory and astrophysical plasmas. For example, Welch *et al*., [13] used it (with the constant in the right side of Eq. (50) suggested by Griem [19]) for determining the electron density in the low-density discharge at Alcator *C*-Mod.

However, in magnetized plasmas the Lorentz field E_L can significantly exceed the most probable Holtsmark field $E_{\max}$, as shown in Sect. 2. In this situation the number $n_{\max}$ of the last observable hydrogen line will not be controlled by the electron density, but rather by different parameters, as shown below. Let us first conduct a simplified reasoning along the approach of Inglis and Teller [10]. By substituting $E = E_L$ in the left side of Eq. (49), we obtain the following relation

$$n_{\max}^{10} B^2 T(K) = 1.78 \times 10^{18} M/M_p \quad \text{or} \quad n_{\max}^{10} B^2 T(eV) = 1.54 \times 10^{14} M/M_p, \tag{51}$$

where B is the magnetic field in Tesla; M and M_p are the atomic and proton masses, respectively.

More accurate relations can be derived using the results of our calculations of Lorentz-broadened profiles of high-n Balmer lines and the corresponding formulas (43)-(46) for the sum of the half widths at half maximum of two adjacent Balmer lines. In this more accurate way we obtained the following relations.

For the observation perpendicular to **B**:

$$n_{\max}^{10} B^2 T(K) = 2.79 \times 10^{18} M/M_p \quad \text{or} \quad n_{\max}^{10} B^2 T(eV) = 2.40 \times 10^{14} M/M_p. \tag{52.A}$$

For the observation parallel to **B**:

$$n_{\max}^{10} B^2 T(K) = 1.78 \times 10^{18} M/M_p \quad \text{or} \quad n_{\max}^{10} B^2 T(eV) = 1.54 \times 10^{14} M/M_p. \tag{52.B}$$

For the "isotropic" case (the meaning of which was explained after Eq. (46)):

$$n_{\max}^{10} B^2 T(K) = 2.38 \times 10^{18} M/M_p \quad \text{or} \quad n_{\max}^{10} B^2 T(eV) = 2.05 \times 10^{14} M/M_p. \tag{52.C}$$

Thus, the above formulas, by using the observable quantity $n_{\max}$, allow to measure the atomic temperature T, if the magnetic field is known, or the magnetic field B, if the temperature is known. The accuracy can be increased by taking into account additional broadening mechanisms as follows

$$[(\Delta\omega_{1/2}(n))^2 + \Delta\omega_Z^2 + (\Delta\omega_D)_{1/2}^2]^{1/2} = m_e e^4/(n^3 \hbar^3), \tag{53}$$

where the sum $\Delta\omega_{1/2}(n)$ of Lorentz halfwidths of the two adjacent high-n Balmer lines, the Zeeman width $\Delta\omega_Z$, and the Doppler width $(\Delta\omega_D)_{1/2}$ are given by Eqs. (47), (11), and (33), respectively.

We also note that the Lorentz and Zeeman mechanisms can be combined together "exactly" using the fact that the problem of a hydrogen atom in the crossed electric and magnetic fields allows an analytical solution which is exact within the subspace spanned on the states of the principal quantum number n. This fact, being the consequence of the $O(4)$ symmetry of the hydrogen atom (and of the corresponding Kepler problem), was presented already in 1927 by Born in frames of the "old quantum theory" [20] and was later elaborated in more detail in the contemporary quantum theory by Demkov, Monozon, and Ostrovsky [21]. The characteristic frequencies, arising in this solution, are $\xi\Omega$, where

$$\Omega = \{[\Delta\omega_L/(n-1)]^2 + \Delta\omega_Z^2\}^{1/2}, \qquad \xi = -(n-1), -(n-2), \ldots, (n-1), \tag{54}$$

$\Delta\omega_L$ and $\Delta\omega_Z$ being given in Eq. (11). It is seen that the characteristic frequencies $\xi\Omega$ are similar to the left side of Eq. (53) if in the latter the Doppler broadening would be disregarded.

For example, for the low-density discharge at Alcator *C*-Mod [13], where deuterium Balmer lines up to $n_{\max} = 16$ were observed and the magnetic field was $B = 8$ Tesla, we obtain from Eq. (53): $T = 6$ eV.

Another example: in solar chromosphere, where Balmer lines up to $n_{\max} \sim 30$ have been observed, assuming $T \sim 10^4$ K and the average non-thermal velocity $v_{\text{nonth}} \sim 20$ km/s, we obtain from Eq. (53): $B \sim 0.2$ Tesla.

4. LORENTZ-DOPPLER BROADENING OF HIGHLY-EXCITED HYDROGEN LINES

In this section we make an allowance for the Doppler broadening. The most prominent feature of the combined Lorentz-Doppler broadening is that it does not reduce to the convolution of Lorentz and Doppler broadenings, as first noted by Galushkin [1]. These two broadening mechanisms entangle in a more complicated way because in the laboratory reference frame, the Lorentz-Doppler profile of a Stark component of a hydrogen line is proportional to the following δ-function (in the frequency scale) $\delta[\Delta\omega - (\omega_0 v/c)\cos\alpha - (kX_{\alpha\beta}Bv/c)\sin\theta]$, where α is the angle between the direction of observation and the atomic velocity **v**, and θ is the angle between vectors **v** and **B**.

For obtaining the results in the most universal way, we use the following dimensionless notations,

$$w = c\,\Delta\omega/(v_T\omega_0) = c\,\Delta\lambda/(v_T\lambda_0), \qquad \mathbf{b} = kX_{\alpha\beta}\mathbf{B}/\omega_0, \qquad \mathbf{u} = \mathbf{v}/v_T, \tag{55}$$

where w is the scaled detuning from the unperturbed frequency or from the unperturbed wavelength of a hydrogen spectral line, **b** is the scaled magnetic field, and **u** is the scaled atomic velocity. The quantities k and $X_{\alpha\beta}$ were defined in Eq. (20).

We start from the situation where the direction of the observation is along **B**. This case has never been studied (to the best of our knowledge). In this case, the Lorentz-Doppler profile of a Stark component of a hydrogen line can be expressed as follows

$$I_{\text{par}}(w, b) = \int_0^\infty du\, f(u) \int_0^1 d(\cos\theta)\,\delta(w - u\cos\theta - b\sin\theta), \tag{56}$$

where the velocity distribution $f(u)$ is usually taken as the Maxwell distribution

$$f(u) = (4u^2/\pi^{1/2})\exp(-u^2). \tag{57}$$

For brevity we denote $\cos\theta = x$. The root x_0 of the argument of the δ-function in Eq. (56) is

$$x_0(u, b) = [u - b(1 + b^2 - u^2)^{1/2}]/(1 + b^2). \tag{58}$$

Using the properties of the δ-function, Eq. (56) can be reduced to

$$I_{\text{par}}(w, b) = (2/\pi^{1/2}) \int_{y_{\min}}^\infty dy\, y \exp(-y^2)/\{1 - bx_0(w/y, b)/[1 - x_0^2(w/y, b)]^{1/2}\}, \tag{59}$$

where y_{min} is given as follows. For $b > 0$:

$$y_{min} = w/(1 + b^2)^{1/2} \quad \text{for} \quad w > 0, \qquad y_{min} = -w \quad \text{for} \quad w < 0. \tag{60}$$

For $b < 0$:

$$y_{min} = w/(1 + b^2)^{1/2} \quad \text{for} \quad w < 0, \qquad y_{min} = -w \quad \text{for} \quad w > 0. \tag{61}$$

Figures 2 and 3 show the Lorentz-Doppler profile from Eq. (59) for the scaled magnetic field $b = 0.2$ and $b = 1$, respectively. For comparison, the corresponding pure Doppler profile is also shown in these Figures. Figure 4 shows the Lorentz-Doppler profile from Eq. (59) for a larger the scaled magnetic field $b = 10$.

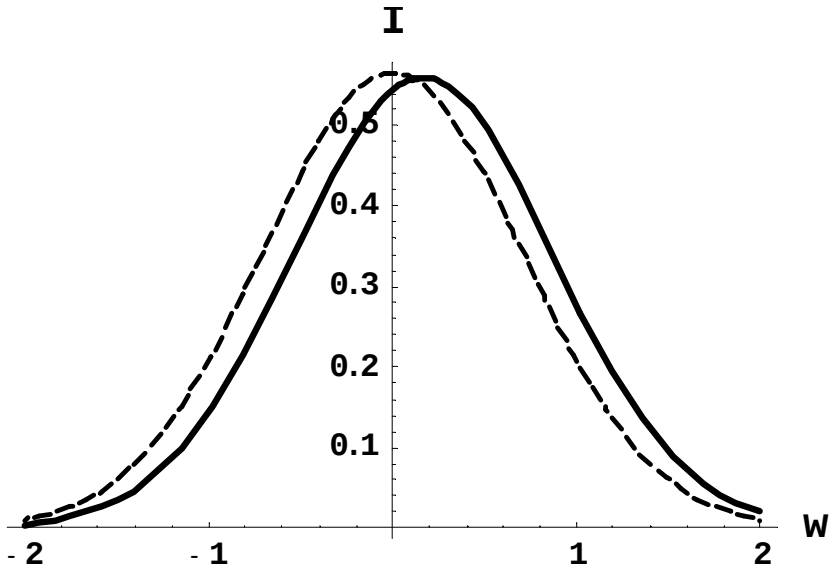

Figure 2: The Lorentz-Doppler profile from Eq. (59) for the scaled magnetic field $b = 0.2$ (solid line). For comparison, the corresponding pure Doppler profile is also shown (dashed line). The direction of observation is parallel to the magnetic field B

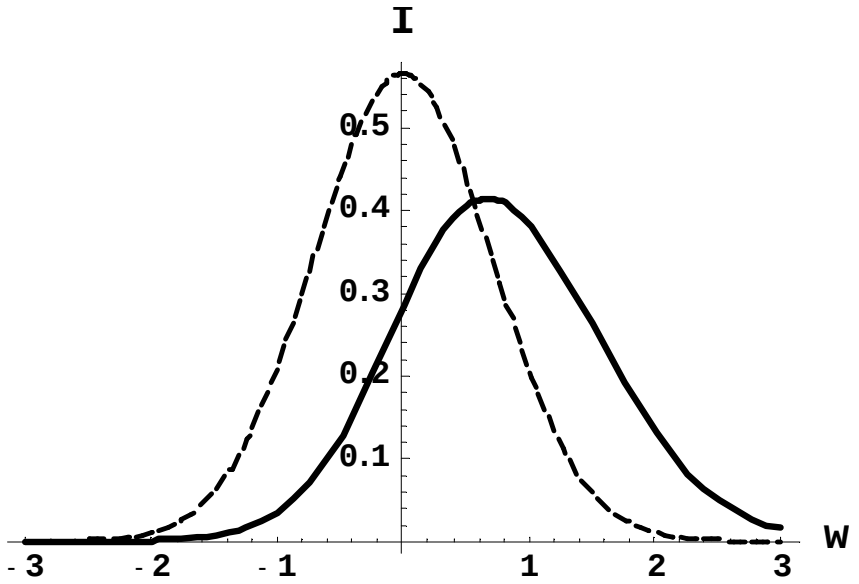

Figure 3: The same as in Fig. 2, but for the scaled magnetic field $b = 1$

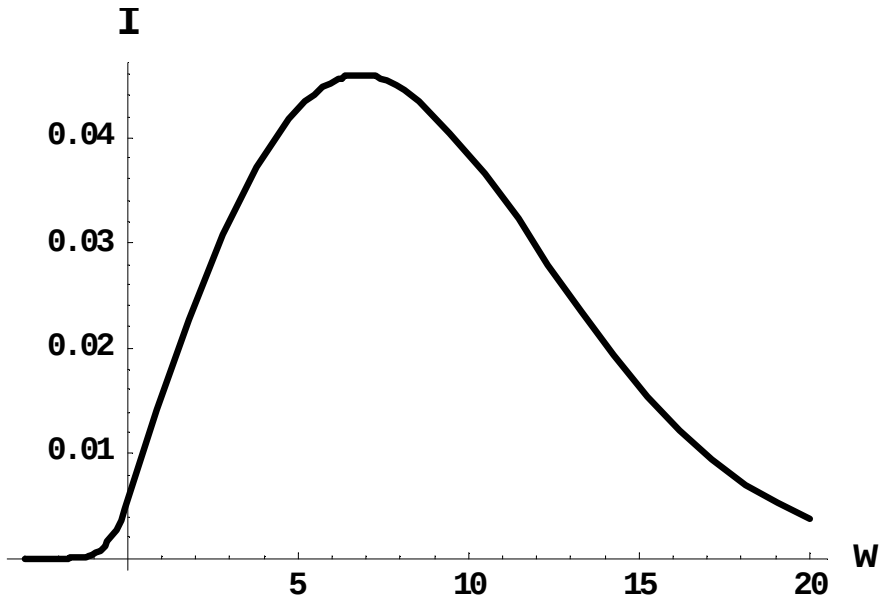

Figure 4: The Lorentz-Doppler profile from Eq. (59) for the scaled magnetic field $b = 10$. The direction of observation is parallel to the magnetic field B**.**

It is seen that, as the magnetic field increases, the maximum of the profile shifts further away from the unperturbed frequency of the spectral line and the profile becomes more and more asymmetric. However, to avoid any confusion we emphasized that the profiles in Figs. 2-4 are for a Stark component shifted to the blue side, i.e., for a Stark component, for which $X_{\alpha\beta} > 0$ in Eq. (20) so that $b > 0$. For a pair of Stark components, corresponding to two equal by magnitude and opposite by sign values of $X_{\alpha\beta}$ (and consequently, of b), the resulting profile $I(w, b) = I_{\text{par}}(w, b) + I_{\text{par}}(w, -b)]$ is symmetric – see Fig. 5 combining the cases of $b = 10$ and $b = -10$.

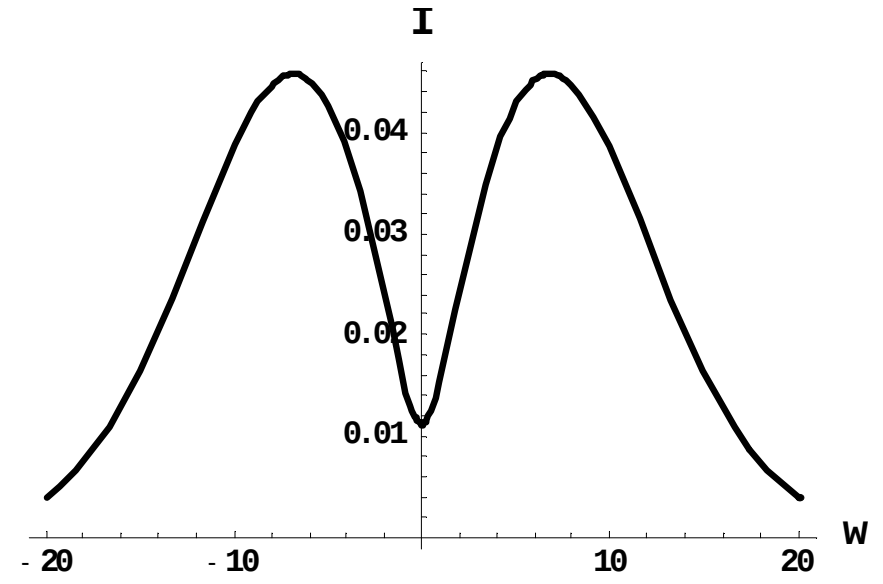

Figure 5: The resulting Lorentz-Doppler profile for a pair of Stark components, corresponding to two equal by magnitude and opposite by sign values of $X_{\alpha\beta}$ (in Eq. (20)). Specifically, it is the combined profile corresponding to the cases of $b = 10$ and $b = -10$

We note that for large magnetic fields ($b >> 1$), the combined profile of such two Stark components closely resembles the shape of the pure Lorentz-broadened profile symmetrized as $S_{\alpha\beta}(\Delta\omega) + S_{\alpha\beta}(-\Delta\omega)$, where $S_{\alpha\beta}(\Delta\omega)$ is given by Eq. (34).

Based on the universal function $I_{\rm par}(w, b)$ from Eq. (59), the profiles $S(\Delta\omega)$ of hydrogen lines in the frequency scale can be calculated as follows (for the observation along **B**)

$$S(\Delta\omega) = S_{\pi}(\Delta\omega) + S_{\sigma}(\Delta\omega), \tag{62}$$

$$S_{\pi}(\Delta\omega) = [c/(v_T\,\omega_0)] \sum_{(\alpha,\beta)\pi} J_{\alpha\beta}\, f_{\pi}\, I_{\rm par}[c\,\Delta\omega/(v_T\,\omega_0)], \tag{63}$$

$$S_{\sigma}(\Delta\omega) = [c/(v_T\,\omega_0)] \sum_{(\alpha,\beta)\pi} J_{\alpha\beta}\, f_{\pi}\, I_{\rm par}[c\,\Delta\omega/(v_T\,\omega_0)], \tag{64}$$

where $f_{\pi} = 1$, $f_{\sigma} = 1/2$ (see Eq. (30)).

For the case of a nonzero angle ψ between the direction of observation and the magnetic field, the relative configuration of the vectors **B**, $\mathbf{E}_L$, and **v**, as well as the choice of the reference frame is shown in Fig. 6.

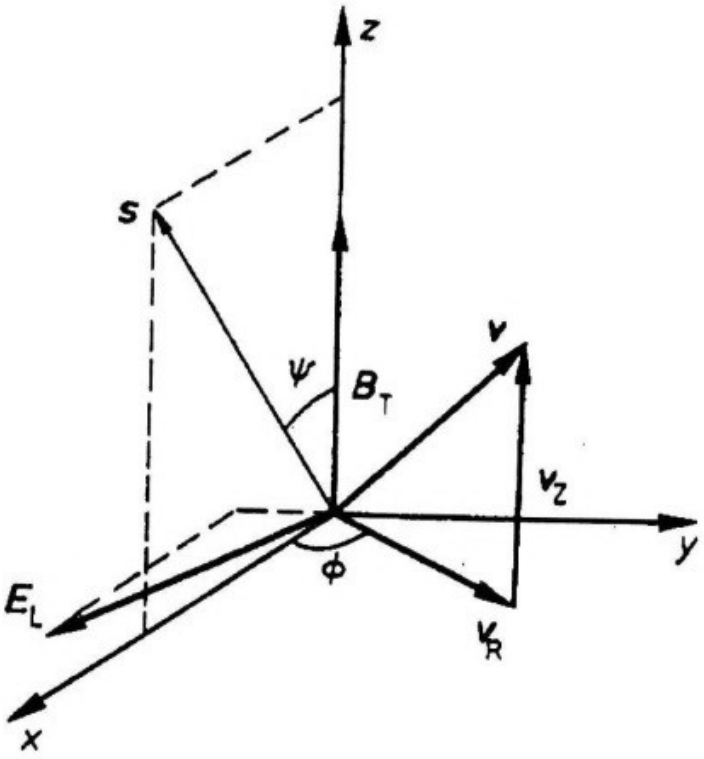

Figure 6: Relative configuration of the magnetic B and Lorentz E_L fields and of the direction of the observation s ("s" stands for "spectrometer"). The z axis is along B. The direction of the observation s constitutes a non-zero angle ø with B. The *xz* plane is spanned on vectors B and s. The atomic velocity v has a component v_z along B and a component v_R perpendicular to B. The component v_R constitutes an angle φ with the *x*-axis

If we would disregard for a moment the angular dependence of the intensities of π- and σ-components of hydrogen lines, then the Lorentz-Doppler profile of a Stark component can be expressed as follows

$$I(w, b) = \int_0^{\infty} du_z\, f_z(u_z) \int_0^{\infty} du_R\, f_R(u_R) \int_0^{1} d(\cos\psi) \int_0^{\pi} (d\varphi/\pi)\, \delta[w - u_z \cos\psi - u_R(b + \sin\psi\cos\varphi)]. \tag{65}$$

Here

$$f_z(u_z) = \pi^{-1/2} \exp(-u_z^2) \tag{66}$$

is the 1-D Maxwell (i,e,. Bolzmann) distribution of the scaled component $u_z = v_z/v_T$ of the atomic velocity parallel to **B**, and

$$f_R(u_R) = 2u_R \exp(-u_R^2) \tag{67}$$

is the 2-D Maxwell distribution of the scaled component $u_R = v_R/v_T$ of the atomic velocity perpendicular to **B**.

For allowing for the angular dependence of the intensities of π- and σ-components, the corresponding angular factors (as functions of ψ) should be entered in Eq. (65) into the integral over $d(\cos\psi)$. For example, for the simplest case, where only the component of the radiation polarized along **B** is observed, this factor is $\sin^2\psi$. Of course, such component of the radiation is only one part of the corresponding σ-Stark-component of the hydrogen line.

For obtaining more specific results, we consider below the case of the observation perpendicular to **B**, i.e., the case of $\psi = \pi/2$. In this case, Eq. (65) reduces to:

$$I_{\rm per}(w, b) = \int_0^\infty du_R f_R(u_R) \int_0^\pi (d\varphi/\pi)\, \delta[w - u_R(b + \cos\varphi)]. \tag{68}$$

For the subcase of $|b| < 1$, using the properties of the δ-function, Eq. (65) can be simplified to:

$$I_{\rm per}(w, b) = [\pi(1 - b)^{1/2}]^{-1} \int_{u_{R_{\rm min}}}^\infty du_R\, 2u_R \exp(-u_R^2)/\{[u_R - w/(1 + b)][u_R + w/(1 - b)]\}^{1/2}. \tag{69}$$

For $0 < b < 1$:

$$u_{R_{\rm min}} = w/(1 + b) \quad \text{for} \quad w > 0, \qquad u_{R_{\rm min}} = -w/(1 - b) \quad \text{for} \quad w < 0. \tag{70}$$

For $-1 < b < 0$:

$$u_{R_{\rm min}} = -w/(1 - b) \quad \text{for} \quad w > 0, \qquad u_{R_{\rm min}} = w/(1 + b) \quad \text{for} \quad w > 0. \tag{71}$$

We note that an expression equivalent to our Eq. (69) was previously obtained by Breton *et al*., [3]. However, in [3] the lower limit of the integration was set (in our notations) to $u_{R_{\rm min}} = w/(1 + b)$ regardless of the sign of b and of the sign of the scaled detuning w from the unperturbed position of the spectral line. Therefore, their calculations of the profiles of the H_α and H_β lines seem to contain errors.

Equation (69) yields the spectral line profile for the simplest case, where only the component of the radiation polarized along **B** is observed. Such component of the radiation is only one part of the corresponding σ-Stark-component of the hydrogen line, as mentioned above. For allowing for the angular dependence of the intensities of π- and σ-components, the following factors should be entered in Eq. (69) into the integral over du_R:

$$(b - w/u_R)^2 \text{ for } \pi\text{-components}, \qquad [(1 - b^2/2)u_R^2 + bwu_R - w^2/2]/u_R^2 \text{ for } \sigma\text{-components}. \tag{72}$$

Now we proceed to the subcase of $|b| > 1$. Using the properties of the δ-function, Eq. (65) can be simplified as follows.

For $b > 1$ and $w > 0$:

$$I_{\rm per}(w, b) = [\pi(1 - b)^{1/2}]^{-1} \int_{u_{R_{\rm min}}}^{u_{R_{\rm max}}} du_R\, 2u_R \exp(-u_R^2)/\{[w/(b - 1) - u_R][u_R - w/(b + 1)]\}^{1/2}, \tag{73}$$

where

$$u_{R_{\rm min}} = w/(1 + b), \qquad u_{R_{\rm max}} = w/(b - 1). \tag{74}$$

For $b > 1$ and $w < 0$, or for $b < -1$ and $w > 0$:

$$I_{\rm per}(w, b) = 0. \tag{75}$$

For $b < -1$ and $w < 0$:

$$I_{\rm per}(w, b) = [\pi (1 - b)^{1/2}]^{-1} \int_{u_{R_{\min}}}^{u_{R_{\max}}} du_R\, 2u_R \exp(-u_R^2)/\{[w/(b + 1) - u_R][u_R - w/(b - 1)]\}^{1/2}, \tag{76}$$

where

$$u_{R_{\min}} = w/(b - 1), \qquad u_{R_{\max}} = w/(1 + b). \tag{77}$$

Similarly to the subcase of $|b| < 1$, in the subcase of $|b| > 1$, Eqs. (73), (76) yield the spectral line profile for the simplest situation, where only the component of the radiation polarized along **B** is observed. For allowing for the angular dependence of the intensities of π- and σ-components, the corresponding factors given by Eq. (72) should be entered in Eqs. (73), (76) into the integral over du_R.

Finally we consider the remaining subcase of $|b| = 1$. Using the properties of the δ-function, Eq. (65) can be simplified as follows.

For $b = 1$ and $w > 0$, or for $b = -1$ and $w < 0$:

$$I_{\rm per}(w) = (\pi |w|)^{-1} \int_{|w|/2}^{\infty} du_R\, 2u_R \exp(-u_R^2)/(u_R - |w|/2)^{1/2}. \tag{78}$$

The integral in Eq. (78) can be calculated analytically, so that Eq. (78) takes the form

$$I_{\rm per}(w) = [\Gamma(1/4)\Gamma(-1/4)|w|]^{-1}[\Gamma(-1/4) F(3/4, 1/2; -w^2/4) - \Gamma(1/4)|w| F(5/4, 3/2; -w^2/4)], \tag{79}$$

where $\Gamma(z)$ is the gamma-function, $F(\alpha, \gamma; z)$ is the confluent hypergeometric function.

For $b = 1$ and $w < 0$, or $b = -1$ and $w > 0$:

$$I_{\rm per}(w) = 0. \tag{80}$$

Similarly to the subcases of $|b| < 1$ and $|b| < 1$, in the subcase of $|b| = 1$, Eqs. (78) yields the spectral line profile for the simplest situation, where only the component of the radiation polarized along **B** is observed. For allowing for the angular dependence of the intensities of π- and σ-components, the corresponding factors given by Eq. (72), with the substitution of $b = 1$ or $b = -1$, should be entered in Eqs. (78) into the integral over du_R.

Finally we emphasize that the above results for the subcases of $|b| > 1$ and $|b| = 1$ have never been presented in the literature – to the best of our knowledge.

5. CONCLUSIONS

We presented several new aspects concerning magnetized plasmas where the Lorentz broadening of hydrogen (or deuterium, or tritium) spectral lines is significant. For plasmas containing a low-frequency electrostatic turbulence we derived analytically distributions of the total electric field and the corresponding Stark profiles of hydrogen lines. This kind of turbulence causes anomalous transport phenomena (e.g., the anomalous resistivity) and is therefore very important to be diagnosed in magnetized plasmas.

Second, for non-turbulent magnetized plasmas we derived analytically Lorentz-broadened profiles of highly-excited hydrogen lines. We obtained formulas for the principal quantum number $n_{\max}$ of the last observable hydrogen line in the spectral series. These formulas differ very significantly from the corresponding Inglis-Teller result and constitute a new diagnostic method allowing to measure the product $T^{1/2}B$, where T is the atomic temperature. In other words, this method allows measuring the atomic temperature T, if the magnetic field is known, or the magnetic field B, if the temperature is known.

Third, we discussed Lorentz-Doppler broadening of highly-excited hydrogen lines. These two broadening mechanisms entangle in a more complicated way than a simple convolution. We produced several new analytical results.

We demonstrated that our findings lead to a significantly revised interpretation of the previous and future experimental/observational data at least in two research areas. One of the research areas is magnetic fusion, i.e., controlled thermonuclear fusion based on a magnetic confinement of the fuel plasma. The other research area is solar physics.

References

[1] Yu. I. Galushkin, *Sov. Astron*., **14**, (1970), 301.

[2] R. C. Isler, *Phys. Rev. A*, **14**, (1976), 1015.

[3] C. Breton, C. De Michelis, M. Finkental, and M. Mattioli, *J. Phys. B: Atom. Mol. Phys*., **13**, (1980), 1703.

[4] Nguen Hoe, J. Crumbers, M. Caby, E. Leboucher, and G. Couland, *Phys. Rev.* ***A***, **24**, (1981), 438.

[5] S Brilliant, G. Mathys, and C. Stehle, *Astron. Astrophys*., **339**, (1998), 286.

[6] C. Stehle, S. Brilliant, and G. Mathys, *Eur. Phys. J. D*, **11**, (2000), 491.

[7] V. N. Tsytovich, *Theory of Turbulent Plasmas*, Consultants Bureau, New York, (1977).

[8] B. B. Kadomtsev, *Plasma Turbulence*, Academic, New York, (1965).

[9] *Turbulence and Anomalous Transport in Magnetized Plasmas*, Proc. Int. Workshop at "Institut d'Etudes Scientifiques de Cargese", Corse de Sud, France, Edits. D. Gresillon and M. A. Dubois, Editions de Physique, Les Ulis, France, (1987).

[10] D. R. Inglis, and E. Teller, *Astrophys. J*., **90**, (1939), 439.

[11] E. Oks, in "*Atomic Processes in Basic and Applied Physics*", 2012, Springer Series on Atomic, Optical and Plasma Physics, Springer, New York, **68**, 393-432.

[12] J. Holtsmark, *Ann. Phys*., **58**, (1919), 577.

[13] B. L. Welch, H. R. Grim, J. Terry, C. Kurz, B. LaBombard, B. Lipschultz, E. Maramar, and G. McCracken, *Phys. Plasmas*, **2**, (1995), 4246.

[14] V. P. Gavrilenko, E. Oks, and V. A. Rantsev-Kartinov, *JETP Letters*, **44**, (1986), 404.

[15] F. D. Rosenberg, U. Feldman, and G.A. Doschek, *Astrophys. J*., **212**, (1977), 905.

[16] U. Feldman and G. A. Doschek, *Astrophys. J*., **212**, (1977), 913.

[17] G. V. Sholin and E. Oks, *Sov. Phys. Doklady*, **18**, (1973), 254.

[18] J. Hey, *J. Phys. B: At. Mol. Opt. Phys*., **46**, (2013), 175702.

[19] H. R. Griem, *Plasma Spectroscopy*, McGraw-Hill, New York, (1964).

[20] M. Born, *The Mechanics of the Atom*, Bell and Sons, London, (1927).

[21] Yu. N. Demkov, B. S. Monozon, and V. N. Ostrovsii, *Sov. Phys. JETP*, **30**, (1970), 775.